Available online at www.sciencedirect.com
ScienceDirect
International Journal of Heat and Mass Transfer 50 (2007) 2296–2308
International Journal of HEAT and MASS TRANSFER
www.elsevier.com/locate/ijhmt

Heat transfer with flow and evaporation in loop heat pipe's wick at low or moderate heat fluxes

Chuan Ren, Qing-Song Wu *, Mao-Bin Hu

Department of Thermal Science and Energy Engineering, University of Science and Technology of China, Hefei, Anhui 230026, China

Received 27 November 2005; received in revised form 21 August 2006
Available online 11 January 2007

Abstract

An axisymmetric two-dimensional mathematical model of the cylindrical evaporator's wick of loop heat pipes is developed to simulate heat transfer with flow and evaporation in the capillary porous structure. Effect of the interaction between the flow field and the liquid–vapor interface on the position of the interface and the curvature of menisci is adequately considered in this model. The flow fields of transient and steady states are obtained at low or moderate heat fluxes. The dynamic and thermodynamic behavior is discussed in this paper. The auto-driving mechanism of "inverted meniscus type" evaporators is validated. Effect of heat flux is investigated in detail.

Keywords: Loop heat pipe; Axisymmetric; Capillary porous structure; Heat transfer; Evaporation

1. Introduction

The loop heat pipe (LHP) is a two-phase thermal control device with the capillary pump driving a working fluid to flow and transfer heat over long distance, just as the capillary pumped loop (CPL). Due to their growing application to many engineering domains including thermal management of satellites and spacecrafts as well as cooling of electrical and electronic devices, researches to CPLs/LHPs become more active and important in the last decade after the researches were revealed in public in 1991 [1–8]. Kaya and Hoang [1,2] numerically simulated and experimentally validated the steady-state performance of a LHP, Hoang and Ku [3] made researches of hydrodynamic aspects of CPLs, Ku [4] investigated operating characteristics of LHPs, Pouzet et al. [5] investigated dynamic response of a CPL at various heat loads, Zhang et al. [6] focused on startup behavior of a LHP. Vasiliev [7] and Maydanik [8] reviewed the researches to LHPs in 2005. Most of the previous researches focused on tests or simulation of the whole device, many important properties of evaporators are neglected. The evaporator with the capillary porous structure is the primary functional component which accepts heat fluxes, organizes evaporation and produces driving force of the working fluid flowing circularly in the whole device. Heat transfer with flow and evaporation occurs just in the capillary porous structure. For the security and efficiency of LHPs performance, it is important and necessary to investigate the dynamic and thermodynamic behavior of the working fluid in the capillary porous structure and the auto-driving mechanism of the "inverted meniscus type" evaporator, which was first introduced and used in a heat pipe by Feldman and Noreen [9].

Khrustalev and Faghri [10] developed a one-dimensional mathematical model on the basis of heat transfer with thin-film evaporation theory in a pore and heat transfer in the dry porous media and close-touched heated fins (or flat), and the analytical steady solution was derived. It was proved that there lies a steady vapor blanket between the liquid-saturated zone in porous media and close-touched heated fins (or flat) for a definite interval of heat fluxes. Zhao and Liao [11] investigated experimentally heat

---

[*] Corresponding author. Tel.: +86 5513601272; fax: +86 5513606459.
E-mail address: qswu@ustc.edu.cn (Q.-S. Wu).

0017-9310/$ - see front matter © 2006 Elsevier Ltd. All rights reserved.
doi:10.1016/j.ijheatmasstransfer.2006.10.029

Nomenclature

A_s	the area of a close-contacted heated fin, m^2
c	special thermal capacity, J/(kg K)
h	enthalpy, J/kg
k	thermal conductivity, W/(m K)
K	permeability, m^2
$\dot{m}$	flux of the working fluid, kg/s
$\mathbf{n}$	normal vector on the liquid–vapor interface
p	pressure, Pa
q	heat flux, W/m^2
$\mathbf{r}$	position vector of meniscus, m
R	radii of meniscus' curvature, m
R_M	gas constant, J/(kg K)
$\mathbf{s}$	displacement vector of interface, m
t	time, s
T	temperature, K
U	total heat transfer coefficient, $W/(m^2 K)$
$\mathbf{V}$	velocity vector of infiltration, m/s

Greek symbols

ϕ	porosity
β_T	expansion coefficient with constant pressure, 1/K
β_p	expansion coefficient with constant temperature, 1/Pa
λ	latent heat of evaporation, J/kg
μ	dynamic viscosity, kg/(m s)
ν	kinematic viscosity, m^2/s
ρ	density, kg/m^3
σ	coefficient of surface tension, N/m

Subscripts

c	capillary
e	reference
eva	evaporation
f	fluid
g	vapor
in	on the entrance/inlet
l	liquid
n	normal direction
out	on the exit/outlet
r	in radial direction
s	saturated
t	total
wall	on the heated wall
z	in longitudinal direction

transfer in glass-bead-packed cubic porous media with a groovy heated wall on the top at different heated fluxes, and the one-dimensional approximate solutions derived from this paper agreed with the experimental results. It was indicated that no macroscopic vapor zone was visually observed at low (or moderate) heat fluxes. Demidov and Yatsenko [12], Figus et al. [13], and Takahashi et al. [14] developed two-dimensional steady mathematical models and investigated numerically capillary-driven flow and heat transfer in rectangular porous media, where the study of [12] was in the case of a constant temperature on the top heated boundary with convection and the studies of [13,14] were in the cases of a constant heat flux on the top heated boundary without convection.

Although there have been many studies in this field as mentioned above, three shortcomings exist in current researches. Firstly, current researches to CPLs/LHPs focus on transient characters [5,6,8] and the previous works in literatures stayed at the simulation or experiments of steady heat transfer in the capillary wick [10–14]. Steady mathematical models cannot simulate the development of flow field in porous media from start-up to a steady working state or the response of flow field on the transition between different steady working states. Secondly, the literatures only considered the interaction between the flow field and the position of the liquid–vapor interface in porous media but not the interaction between the flow field and the curvature of menisci, i.e. the capillary force [12–14]. It was always assumed that the capillary force was equal to the maximum capillary force allowed by menisci. Furthermore, the literatures assumed that the vapor on the liquid–vapor interface was saturated and obeyed Clausius–Clapeyron equation, so tracing the liquid–vapor interface could be realized by Clausius–Clapeyron equation [12,13] or the mass transport equation on the interface [14]. However [15,16] pointed out that both vapor and liquid on the liquid–vapor interface are overheated and that the capillary force changes the liquid–vapor thermodynamic equilibrium, which is presented in Kelvin equation. Thirdly, the simulation mainly focused on the cubic porous structures whereas the simulation of the cylindrical porous structure, which is fixed as wicks in most evaporators, was scarce.

In this paper, an axisymmetric two-dimensional mathematical model of the cylindrical evaporator's wick with azimuthal vapor grooves of LHPs is developed to simulate heat transfer with flow and evaporation in the capillary porous structure. Effect of the interaction between the flow field and the liquid–vapor interface on the position of the interface and the curvature of menisci is adequately considered in this model. Effect of heat flux on steady state is investigated in detail.

2. Mathematical model

The evaporator of 16 mm in diameter, investigated in this paper, has the primary wick, the secondary wick, eight

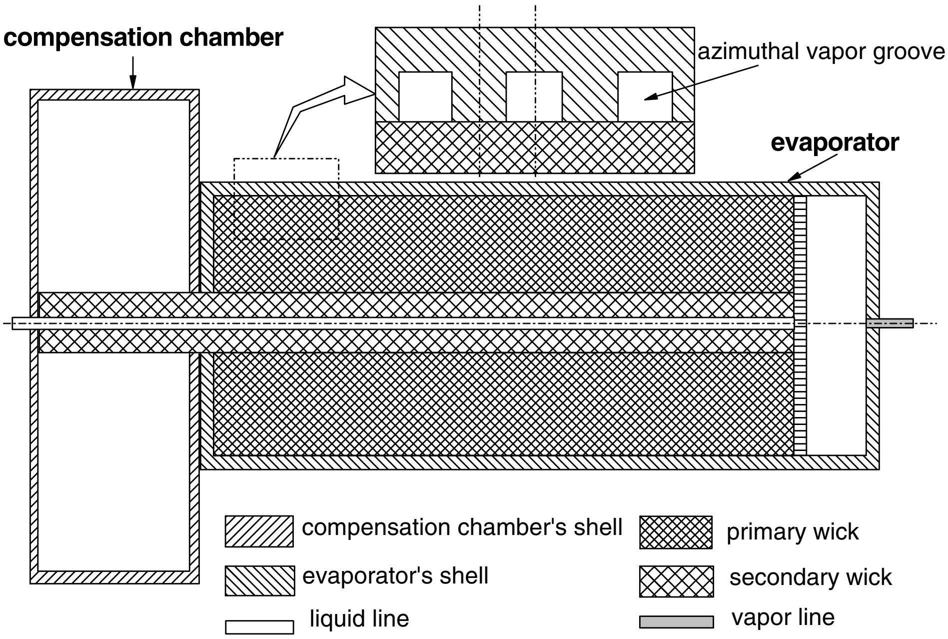

Fig. 1. Configuration of the evaporator with azimuthal grooves and the compensation chamber.

deeper longitudinal grooves and plenty of shallower azimuthal grooves in its shell's wall. The configuration is illustrated in Fig. 1. The primary wick is 5 mm thick in radial direction and it is made of sintered nickel powders with effective pore radius 0.001 mm and porosity 0.5. The permeability, $K = 10^{-13}\ \mathrm{m}^2$, and effective thermal conductivity, $k_{\mathrm{t,l}} = 6.0\ \ \mathrm{W/m\,K}$, are the experimental results of nickel-sintered capillary wick filled with liquid saturating-ammonia. And the effective thermal conductivity of the dry wick, $k_{\mathrm{t,g}}$, is half of it. The width of an azimuthal groove is 1 mm and the width of a heated fin is also 1 mm. In our simulation, a cell shown in Fig. 2 is used to represent the entire primary wick because of the periodic heated boundary on the top and the geometrical and physical symmetry. It is 5 mm thick in radial direction and 1 mm wide in longitudinal direction.

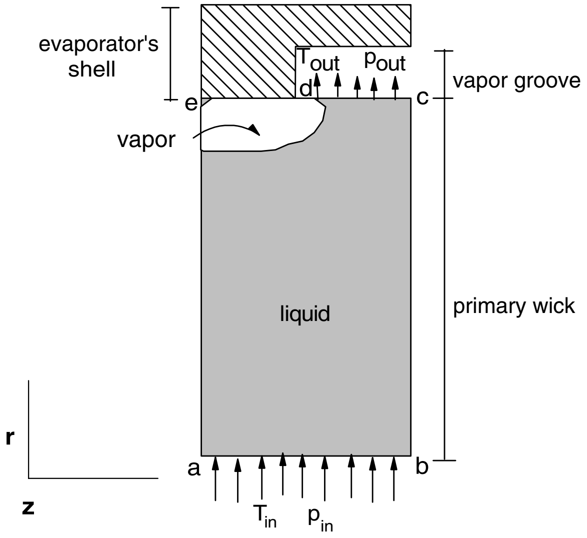

Fig. 2. Diagram of the cell for simulation with the width of half-fin and half-groove.

Some assumptions are introduced: (1) homogeneous, isotropic and rigid capillary porous media, slightly compressible fluids; (2) constant properties for solid, liquid and vapor respectively; (3) gravity, heat radiation and viscous dissipation neglected, no inner heated source; (4) axisymmetric flow to the evaporator's axis and no flow in azimuthal direction; (5) local thermal equilibrium between the solid and fluid phases; (6) evaporation on the liquid–vapor interface, no boiling in liquid.

The mathematical model presented in this paper includes two interactional parts: the model of flow field in porous media and the model of the liquid–vapor interface that is abbreviated as the interface in this paper.

2.1. The model of flow field

The continuum equation of fluid in porous media is the following:

$$\frac{\partial}{\partial t}(\rho_{\mathrm{f}}\phi) + \nabla \cdot (\rho_{\mathrm{f}}\mathbf{V}) = 0, \tag{1}$$

where ϕ is the porosity, ρ_{f} is the density of fluid and $\mathbf{V}$ is the velocity vector of infiltration.

According to the analysis in [17], Darcy's law is able to replace the momentum equation of fluid in porous media even in transient states. So Darcy's law is presented as following with gravity neglected:

$$\mathbf{V} = -\frac{K}{\mu}\nabla p, \tag{2}$$

where K is the permeability, μ is the dynamic viscosity and p is the pressure.

The equation of state is derived as following:

$$\rho_f = \rho_{0,\mathrm{f}}[1 - \beta_{T,\mathrm{f}}(T - T_\mathrm{e}) + \beta_{p,\mathrm{f}}(p - p_\mathrm{e})], \quad \mathrm{f} = \mathrm{l}, \mathrm{g}, \tag{3}$$

where the subscription l and g present liquid and vapor respectively. $\beta_{T,\mathrm{f}}$ is the expansion coefficient with constant pressure and $\beta_{p,\mathrm{f}}$ is the expansion coefficient with constant temperature:

$$\beta_{T,\mathrm{f}} \equiv -\frac{1}{\rho_{0,\mathrm{f}}}\left(\frac{\partial \rho}{\partial T}\right)_p, \quad \beta_{p,\mathrm{f}} \equiv \frac{1}{\rho_{0,\mathrm{f}}}\left(\frac{\partial \rho}{\partial p}\right)_T, \tag{4}$$

where $\beta_{T,\mathrm{g}} = \frac{1}{T}$ and $\beta_{p,\mathrm{g}} = \frac{1}{p}$ when considering vapor as the ideal gas.

Combining (1) with (2) and (3), the pressure equation is derived as following:

$$\phi\frac{\partial}{\partial t}[\rho_{0,\mathrm{f}}\beta_{p,\mathrm{f}}(p - p_\mathrm{e})] - \nabla\cdot\left(\frac{K}{\nu_\mathrm{f}}\nabla p\right) = -\phi\frac{\partial}{\partial t}\{\rho_{0,\mathrm{f}}[1 - \beta_{T,\mathrm{f}}(T - T_\mathrm{e})]\}, \quad \mathrm{f} = \mathrm{l}, \mathrm{g}, \tag{5}$$

where ν_f is the kinematic viscosity. The form of (5) in cylindrical polar coordinates is the following:

$$\frac{\phi}{K}\frac{\partial}{\partial t}[\rho_{0,\mathrm{f}}\beta_{p,\mathrm{f}}(p - p_\mathrm{e})] - \frac{1}{r}\frac{\partial}{\partial r}\left(\frac{r}{\nu_\mathrm{f}}\frac{\partial p}{\partial r}\right) - \frac{\partial}{\partial z}\left(\frac{1}{\nu_\mathrm{f}}\frac{\partial p}{\partial z}\right) = -\frac{\phi}{K}\frac{\partial}{\partial t}\{\rho_{0,\mathrm{f}}[1 - \beta_{T,\mathrm{f}}(T - T_\mathrm{e})]\}. \tag{6}$$

According to the similar deducing process about the energy equation in [17] and the above assumptions, the enthalpy equation for coupled solid and fluid phases is derived as following:

$$\frac{\partial}{\partial t}(\rho_\mathrm{t}h_\mathrm{f}) + \nabla\cdot(\rho_\mathrm{f}\mathbf{V}h_\mathrm{f}) = \phi\frac{\partial p}{\partial t} + \mathbf{V}\cdot\nabla p + \nabla\cdot(k_\mathrm{t}\nabla T), \tag{7}$$

where ρ_t is the total density of coupled solid and fluid phases, k_t is the effective thermal conductivity and h_f is the enthalpy of fluid, which are determined respectively as following:

$$\rho_\mathrm{t} \equiv \phi\rho_\mathrm{f} + (1 - \phi)\rho_\mathrm{s}\frac{c_\mathrm{s}}{c_{p,\mathrm{f}}}, \tag{8a}$$

$$k_\mathrm{t} \equiv \phi k_\mathrm{f} + (1 - \phi)k_\mathrm{s}, \tag{8b}$$

$$h_\mathrm{f} = h_{0,\mathrm{f}} + c_{p,\mathrm{f}}(T - T_\mathrm{e}), \tag{9}$$

where c_s and $c_{p,\mathrm{f}}$ are the specific thermal capacity of solid and fluid, respectively. With temperature replaced by enthalpy, the form of (7) in cylindrical polar coordinates is the following:

$$\frac{\partial}{\partial t}(\rho_\mathrm{t}h_\mathrm{f}) + \frac{1}{r}\frac{\partial}{\partial r}(r\rho_\mathrm{f}V_r h_\mathrm{f}) + \frac{\partial}{\partial z}(\rho_\mathrm{f}V_z h_\mathrm{f}) = \phi\frac{\partial p}{\partial t} + V_r\frac{\partial p}{\partial r} + V_z\frac{\partial p}{\partial z} + \frac{1}{r}\frac{\partial}{\partial r}\left[rk_\mathrm{t}\frac{\partial}{\partial r}\left(\frac{h_\mathrm{f} - h_{0,\mathrm{f}}}{c_{p,\mathrm{f}}}\right)\right] + \frac{\partial}{\partial z}\left[k_\mathrm{t}\frac{\partial}{\partial z}\left(\frac{h_\mathrm{f} - h_{0,\mathrm{f}}}{c_{p,\mathrm{f}}}\right)\right], \tag{10}$$

where V_r and V_z are the velocity of infiltration in radial and longitudinal directions respectively.

The boundary conditions with L_r and L_z presenting the radial thickness and the longitudinal width of a cell respectively are listed in the following. The saturated liquid lies on the entrance with the inlet temperature $T_\mathrm{in} = 293$ K and the inlet pressure $P_\mathrm{in} = 882\,500$ Pa while the outlet pressure P_out is simplified to the value of $P_\mathrm{out} = 882\,500$ Pa.

(1) when $z = 0$ or $z = L_z$ (the boundary b–c and a–e in Fig. 2)

$$\frac{\partial T}{\partial z} = 0, \quad \frac{\partial p}{\partial z} = 0, \tag{11a}$$

(2) when $r = r_\mathrm{in}$ (the boundary a–b in Fig. 2)

$$T = T_\mathrm{in}, \quad p = p_\mathrm{in}, \tag{11b}$$

(3) when $r = r_\mathrm{out} = r_\mathrm{in} + L_r$ and $0 < z < L_z/2$ (the boundary d–e in Fig. 2)

$$\begin{cases} \frac{\partial p}{\partial r} = 0 \\ \quad \text{if interface does not lie on the boundary d–e,} \\ -\rho_\mathrm{f}\frac{K}{\mu_\mathrm{f}}\frac{\partial p}{\partial r}\Big|_\mathrm{l}\lambda = q - k_\mathrm{t}\frac{\partial T}{\partial r}\Big|_\mathrm{l} \\ \quad \text{if interface lies on the boundary d–e,} \end{cases} \tag{11c}$$

$$\begin{cases} -k_\mathrm{t}\frac{\partial T}{\partial r} = q \\ \quad \text{if interface does not lie on the boundary d–e,} \\ -k_\mathrm{t}\frac{\partial T}{\partial r}\Big|_\mathrm{g} = q \\ \quad \text{if interface lies on the boundary d–e,} \end{cases} \tag{11d}$$

(4) when $r = r_\mathrm{out} = r_\mathrm{in} + L_r$ and $L_z/2 < z < L_z$ (the boundary c–d in Fig. 2)

$$\begin{cases} p = p_\mathrm{out} \\ \quad \text{if interface does not lie on the boundary d–e,} \\ \rho_\mathrm{f}\frac{K}{\mu_\mathrm{f}}\frac{\partial p}{\partial r}\Big|_\mathrm{l}\lambda = k_\mathrm{t}\frac{\partial T}{\partial r}\Big|_\mathrm{l} \\ \quad \text{if interface lies on the boundary d–e,} \end{cases} \tag{11e}$$

$$\begin{cases} \frac{\partial T}{\partial r} = 0 \\ \quad \text{if interface does not lie on the boundary d–e,} \\ \frac{\partial T}{\partial r}\Big|_\mathrm{g} = 0 \\ \quad \text{if interface lies on the boundary d–e,} \end{cases} \tag{11f}$$

where λ is the latent heat of evaporation.

Before start-up, pressure and temperature are homogeneous in the fully liquid-saturated porous medium and the working fluid is saturated and resting.

2.2. The model of interface

The conservation and jump of the variants on the liquid–vapor interface in capillary porous media is listed below:

$$T_g|_{\mathbf{s}(\mathbf{r},t)} = T_l|_{\mathbf{s}(\mathbf{r},t)}, \tag{12a}$$

$$p_g|_{\mathbf{s}(\mathbf{r},t)} - p_l|_{\mathbf{s}(\mathbf{r},t)} = \frac{2\sigma}{R(\mathbf{r},t)}, \tag{12b}$$

$$\rho_g\left(\phi\frac{\mathrm{d}\mathbf{s}(\mathbf{r},t)}{\mathrm{d}t} - \mathbf{V}_g\right)\cdot\mathbf{n} = \rho_l\left(\phi\frac{\mathrm{d}\mathbf{s}(\mathbf{r},t)}{\mathrm{d}t} - \mathbf{V}_l\right)\cdot\mathbf{n}, \tag{12c}$$

$$\rho_g h_g\left(\phi\frac{\mathrm{d}\mathbf{s}(\mathbf{r},t)}{\mathrm{d}t} - \mathbf{V}_g\right)\cdot\mathbf{n} + \left(k_t\frac{\partial T}{\partial n}\right)_g = \rho_l h_l\left(\phi\frac{\mathrm{d}\mathbf{s}(\mathbf{r},t)}{\mathrm{d}t} - \mathbf{V}_l\right)\cdot\mathbf{n} + \left(k_t\frac{\partial T}{\partial n}\right)_l, \tag{12d}$$

where $\mathbf{s}(\mathbf{r},t)$ and $\mathrm{d}\mathbf{s}(\mathbf{r},t)/\mathrm{d}t$, σ and $R(r,t)$ are the displacement and velocity of the interface, the coefficient of surface tension and the radius of menisci's curvature, respectively. (12a), (12c) and (12d) indicate respectively the conservation of temperature, mass and energy on the liquid–vapor interface in capillary porous media with interface moving and fluid convection during evaporation while (12b) presents the jump of pressure at the meniscus because of the capillary force. When it is stable or quasi-stable, (12c) and (12d) with $\mathrm{d}\mathbf{s}(\mathbf{r},t)/\mathrm{d}t$ equal to zero or neglectable are reduced to the well-known expressions as following:

$$\rho_g V_{n,g} = \rho_l V_{n,l}, \tag{12e}$$

$$\left(k_t\frac{\partial T}{\partial n}\right)_g - \left(k_t\frac{\partial T}{\partial n}\right)_l = \rho_l V_{n,l}\lambda. \tag{12f}$$

The capillary force not only drives the working fluid to flow but also changes the liquid–vapor thermodynamic equilibrium, which is presented in Kelvin equation [15,16]:

$$p_g = p_s(T)\exp\left(-\frac{p_c}{\rho_l R_M T}\right), \tag{13}$$

where R_M, p_c and $p_s(T)$ are the gas constant for ammonia, capillary force and saturated pressure with temperature T, respectively. And $p_s(T)$ is determined by Clausius–Clapeyron equation:

$$p_s(T) = p_e\exp\left[\frac{\lambda}{R_M}\left(\frac{1}{T_e} - \frac{1}{T}\right)\right], \tag{14}$$

where p_e and T_e are the reference pressure and temperature, respectively.

By using (12d), the velocity and displacement of the interface are presented as following:

$$\frac{\mathrm{d}s_n}{\mathrm{d}t} = \frac{(\rho_l h_l V_{n,l} - \rho_g h_g V_{n,g}) - \left(k_{t,l}\frac{\partial T}{\partial n}\big|_l - k_{t,g}\frac{\partial T}{\partial n}\big|_g\right)}{\phi(\rho_l h_l - \rho_g h_g)}, \tag{15}$$

$$s_n = s_n^0 + \frac{\mathrm{d}s_n}{\mathrm{d}t}\cdot\Delta t. \tag{16}$$

3. Numerical process

In this model, staggered background mesh of 100 × 20 with local thin grid in radial direction is introduced. The number of local thin grid in a background grid is determined by not the possible position of the liquid–vapor interface but the gradient of temperature near the heated fin which is greater at higher heat flux and requests more thin grids in the background grids. Finite volume method is introduced to discretize the pressure equation (6) and the enthalpy equation (10) respectively in liquid and vapor region while boundary conditions are treated as in [18]. The capillary force is treated as the inner boundary on the basis of (12b). The velocity and temperature on both sides of the interface are joined together by (12c) and (12a), respectively. The discretized Eqs. (6) and (10) are treated separately by SIP (strong implicit procedure) [18] and coupled together in each time step while an explicit front tracking method with (15) and (16) is used. The steady state is reached when the maximum relative change of both pressure and temperature among continuous transient states is less than 10^{-6}.

The numerical procedure for each time step is organized as a sequence of the steps:

(1) The initial fields of pressure, temperature, density and enthalpy are given while the fully liquid-saturated porous medium is given with no meniscus on the interface.
(2) Pressure is calculated with Eq. (6) and boundary conditions (11a)–(11c) and (11e).
(3) Velocities of infiltration are calculated via formula (2).
(4) Enthalpy is calculated with Eq. (10) and boundary conditions (11a), (11b), (11d) and (11f).
(5) Temperature is determined via formula (9).
(6) Density of fluid is calculated via Eq. (3).
(7) Update the properties $\beta_{p,g}$ and $\beta_{T,g}$ in Eq. (3).
(8) The capillary force is calculated via Eqs. (13) and (14).
(9) Goto Step (10) if both pressure and temperature are in convergence, otherwise return to Step (2).
(10) Velocity and displacement of the interface are calculated respectively with formulae (15) and (16).
(11) Properties of fluid are updated according to new position of the interface.
(12) The procedure of this time step finishes and the following time step proceeds until the steady state is reached.

4. Results and discussion

4.1. Flow fields of steady states at low and moderate heat fluxes

The low or moderate heat flux is defined as the heat flux at which evaporation only occurs on the liquid–vapor interface but no boiling occurs in liquid, which is listed in the assumptions as mentioned above. The patterns of steady flow fields at low or moderate heat fluxes are similar qualitatively but there are differences in the magnitude. An example at $q = 20\,000$ W/m^2 is presented in Fig. 3. Pressure

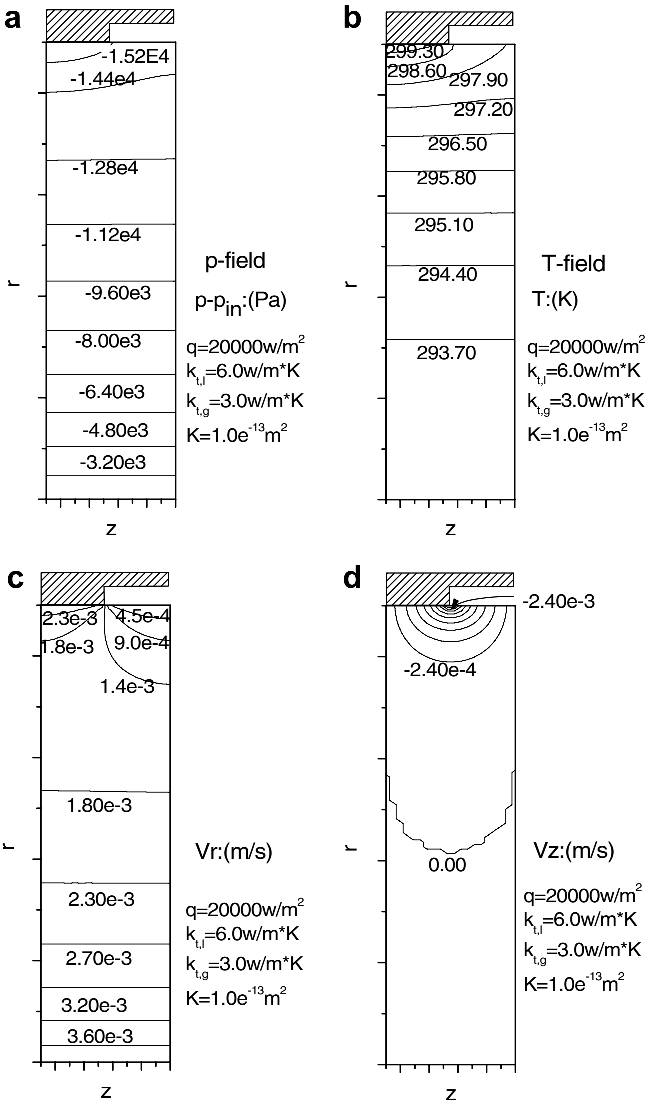

Fig. 3. Isogram of steady state at $q = 20000\ \mathrm{W/m^2}$ (the radial thickness 5 mm and the longitudinal width 1 mm): (a) pressure; (b) temperature; (c) radial velocity; (d) longitudinal velocity.

decreases gradually along radial direction from the entrance to the interface and jumps up suddenly on the interface. Jump of pressure on the interface indicates the capillary force which is the driving force of a LHP. There lies a steady vapor blanket between the liquid-saturated zone in porous media and the close-touched heated fins for a definite interval of heat fluxes [10], but vapor blankets at low or moderate heat fluxes are too thin to be visually observed in experiments [11]. The jump of pressure on the interface and the thickness of thin vapor blankets at low or moderate heat fluxes are shown respectively in Figs. 4–7 with Curves (5) representing those of steady states. Streamlines are perpendicular to isobars. As results of the field of pressure, fluid flows fully in radial direction in most regions of the wick whereas two-dimensional flow only occurs in the vicinity of heated fins and grooves. The radial velocity decreases along radial direction in most regions due to the expansion of flowing area along radial direction, and it increases in the vicinity of heated fins because effect of evaporation is stronger than effect of flowing area expansion.

As shown in Fig. 3b, temperature increases along radial direction from the entrance to the heated fin while there are two-dimensional patterns of isotherms in the vicinity of heated fins and grooves. For a metallic wick with high thermal conductivity, its metallic framework constitutes a channel-net through which heat is diffused from the heat source. So evaporation occurs everywhere on the liquid–vapor interface in porous media including the section far from the heat source where evaporating energy is local heat. The results are coincident to those of [12] and different from those of [13,14] which assumed that no evaporation occurred on the interface between the vapor groove and the liquid-saturated wick. As shown in Figs. 4b and 5b, temperature increases slightly along the boundary c–d, which indicates that there lies a local low-temperature region because of scarce heat. The profile of temperature has steep slope at spot d, which indicates that there lies a thin vapor blanket between the heated fin and the liquid-saturated zone in porous media. Difference of radial velocities on the interface indicates the distribution of evaporative intensity. The closer the region is to the center of the heat source, the more intensely it is vaporizing.

4.2. Development of the flow field and interface in porous media after start-up

Developments of pressure and temperature in the wick after start-up are shown in Fig. 4 at $q = 200\ \mathrm{W/m^2}$ and Fig. 5 at $q = 20000\ \mathrm{W/m^2}$, respectively. Developments of the position of the interface and capillary forces on the interface are shown in Fig. 6 at $q = 200\ \mathrm{W/m^2}$ and Fig. 7 at $q = 20000\ \mathrm{W/m^2}$ respectively. In general, although the interval from start-up to steady state at moderate heat fluxes is longer than that at low heat fluxes, the thermal disturbance at low heat fluxes diffuses more slowly than that at moderate heat fluxes. So the development of pressure and temperature at low heat fluxes may be regarded as the first stage of the development at moderate heat fluxes. By combining the phenomena at low heat fluxes with the phenomena at moderate heat fluxes, we can understand more fully the development of the flow field after start-up.

Heat flux imposed to the evaporator is the sole driving energy of a LHP so that the evaporator starts up as soon as heat flux is imposed to it. The thermal disturbance and evaporation lead to the flow disturbance. As shown in Figs. 4 and 5, after start-up, the thermal disturbance and flow disturbance appear in the vicinity of heat fins firstly, spread to all other regions of the wick with time, and reach the steady state at a certain heat flux finally. Initially, the heat flux only maintains evaporation in the vicinity of heated fins, and evaporation elsewhere is depending on local heat that results in a local low-temperature region there. The vapor produced on the interface close to heated fins is

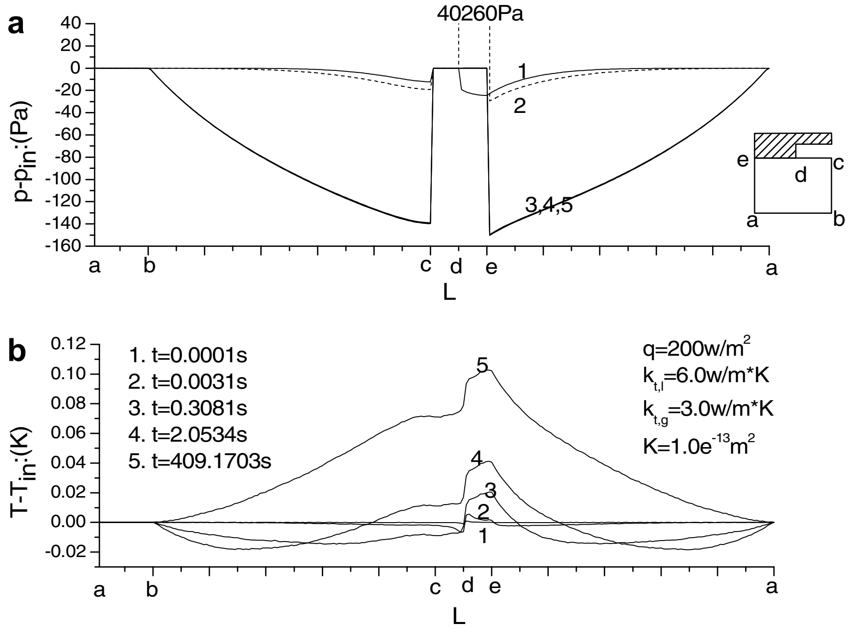

Fig. 4. Profiles of (a) pressure and (b) temperature along boundary with time at $q = 200$ W/m^2.

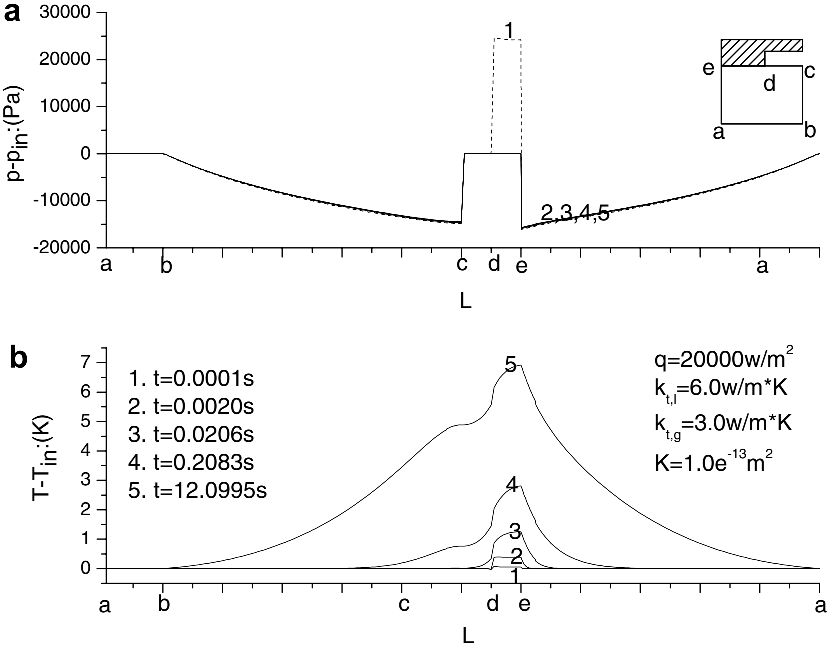

Fig. 5. Profiles of (a) pressure and (b) temperature along boundary with time at $q = 20000$ W/m^2.

constrained in pores of porous media and can not move into vapor grooves. As a result of micro-bubbles in pores appearing, menisci are formed and the difference between vapor pressure and liquid pressure appears to balance the capillary force at menisci. So the jump of pressure, i.e. the pressure difference, is equal to the capillary force. As shown in Figs. 4a, 5a, 6b and 7b, both vapor pressure in micro-bubbles and curvatures of menisci increase with the increment of collected vapor. The pressure and capillary force, which are equal to 40260 Pa, imply that vapor is constrained in pores and the channel to vapor grooves does not exist. And the micro-bubbles expand as soon as capillary forces exceed the maximum capillary force allowed at menisci, until the channel formed to allow vapor moving into vapor grooves. The pressure in the vicinity of heat fins is approximately equal to the outlet pressure, which indicates that the vapor blanket between the liquid-saturated zone and heat fins exists and the vapor is

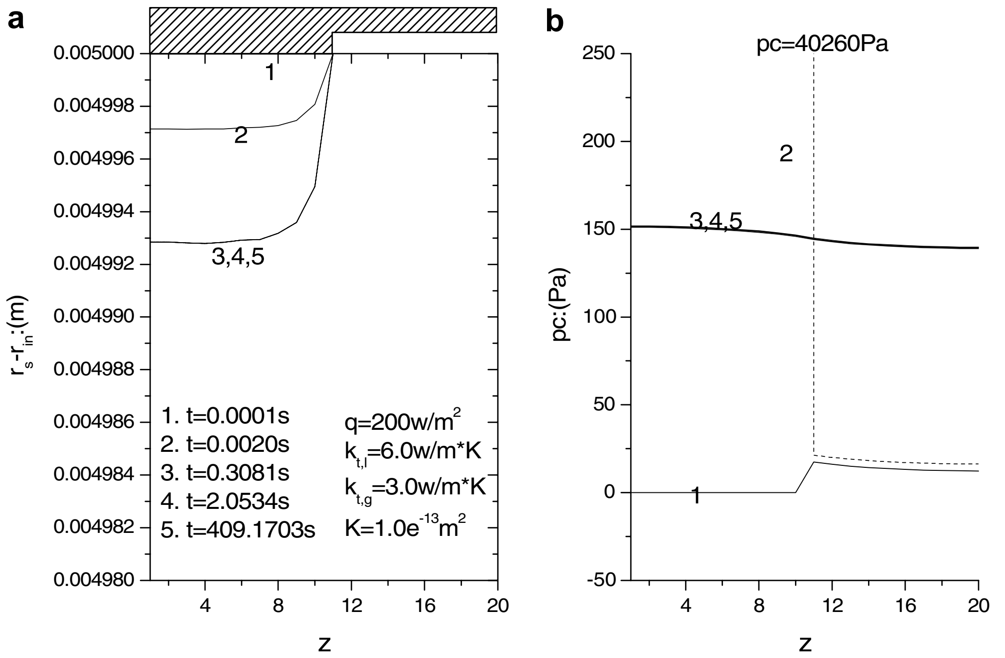

Fig. 6. Development of (a) the position of the interface and (b) capillary forces on the interface at $q = 200\ \mathrm{W/m^2}$.

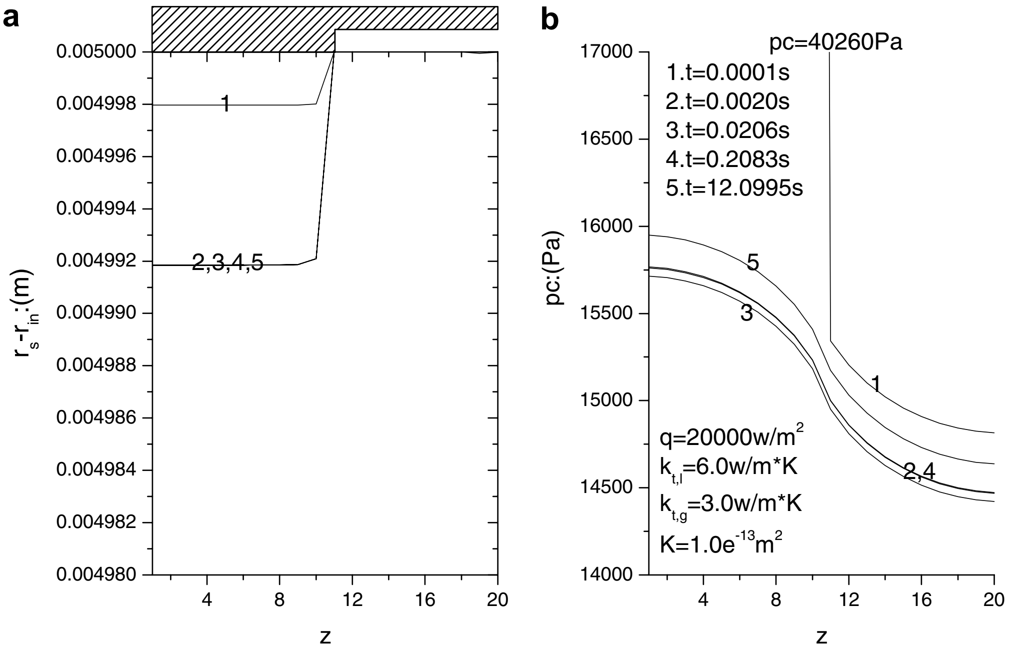

Fig. 7. Development of (a) the position of the interface and (b) capillary forces on the interface at $q = 20000\ \mathrm{W/m^2}$.

no longer constrained in pores. Furthermore, as shown in Figs. 4–7, we can see that pressure and interface develop much faster than temperature.

In capillary porous media, the interface adapts itself to steady states at different heat fluxes automatically by two means: It changes the curvature of menisci or its position in porous media to adjust the flux of the working fluids. The change of the curvature of menisci appears when the curvature of menisci is between the minimum and maximum curvature, and the interface will move when the curvature is greater than the maximum curvature or smaller than the minimum curvature. In point of energy, the transform between the shape-changing potential energy and the kinetic energy exists on the liquid–vapor interface. The potential energy does not transform to the kinetic energy until the total energy of fluid exceeds the maximum of its permitted potential energy [19]. This suggests the possibility of hysteresis in porous media.

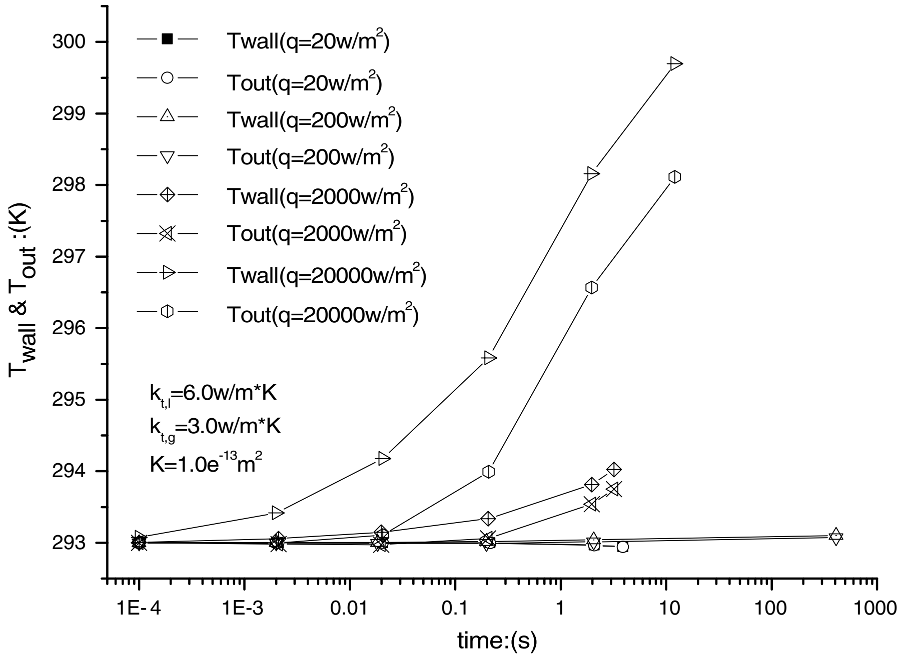

Fig. 8. Development of mean fin temperature T_{wall} and mean outlet temperature T_{out} after start-up with a log scale on time-axis.

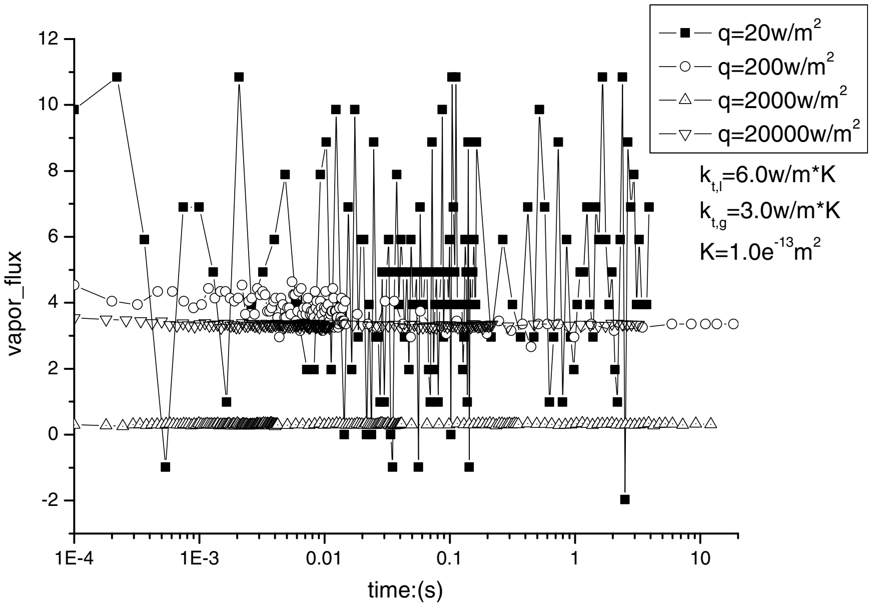

Fig. 9. Development of vapor fluxes after start-up with a log scale on time-axis (vapor_flux $= \frac{\dot{m}}{qA_{\text{s,out}}/\lambda}$. The numerator is the outlet vapor flux calculated by the simulation while the denominator represents the theoretic vapor flux calculated by the balance of energy).

Developments of mean fin temperature T_{wall} and mean outlet temperature T_{out} after start-up at different heat fluxes are shown in Fig. 8. Developments of vapor fluxes on the exit at different heat fluxes are shown in Fig. 9. Note that these time axes in Figs. 8 and 9 are in log coordinate. Both T_{wall} and T_{out} increase with time, as well as the difference between T_{wall} and T_{out} that reaches a certain steady value much earlier than both T_{wall} and T_{out}. Curves of vapor fluxes reach a certain steady value with time except that at $q = 20\ \text{W/m}^2$. Vapor fluxes at moderate heat fluxes develop faster than those at low heat fluxes. The vapor flux at an extremely low heat flux, such as $q = 20\ \text{W/m}^2$, is oscillatory with time, which is explained in next section.

4.3. Influence of different heat fluxes on steady states of a wick

The LHP is a self-driving device depending on heat flux. Heat flux leads to evaporation of the working fluid, and the capillary force at menisci that form because of evaporation of the working fluid in porous media drives the working fluid to flow. This is the auto-driving mechanism of “inverted meniscus type” evaporator, and it is validated in the simulation of development of flow field after start-up. Compared with other effects, heat flux determines primarily the magnitude of pressure and temperature. During heat transfer with flow and evaporation in LHP’s wick, there are three competing dynamic and thermodynamic processes: evaporation, heat conduction of the porous structure and convection of the cool working liquid, among which evaporation occurs only on the interface. The combined effect of the three processes determines pressure, temperature, the position of the interface, the curvature of menisci and so on.

Heat flux, q, obeys the following balance of energy:

$$qA_{\mathrm{s}} = \dot{m}[c_{p,\mathrm{l}}(T_{\mathrm{eva}} - T_{\mathrm{in}}) + \lambda + c_{p,\mathrm{g}}(T_{\mathrm{out}} - T_{\mathrm{eva}})], \tag{17}$$

where A_{s} is the area of a close-contacted heated fin, T_{eva} is evaporating temperature and $\dot{m}$ is the flux of the working fluid. In (17), λ is the latent heat of evaporation and the other two terms in the square brackets is called sensible heat. Combining (2) and (17), considering that sensible heat is much smaller than latent heat, we predict that higher heat flux leads to greater pressure drop and greater capillary force, i.e. the curvature of menisci. As shown in Fig. 10a, profiles of pressure along boundary of steady states at different heat fluxes have the same pattern with different magnitudes. Pressure decreases along radial direction from the entrance to the interface and jumps up on the interface. Jump of pressure is the capillary force. The accelerating of evaporation when heat flux increases leads to the increment of the menisci’s curvature, which drives the working fluid flowing faster in order to compensate the faster evaporation, and the increment of pressure drop in the wick. As shown in Fig. 12b, the capillary force increases monotonously with the heat flux increasing, which increases from 11.6 Pa at $q = 20\ \mathrm{W/m^2}$ to about 40000 Pa at $q = 50000\ \mathrm{W/m^2}$. The numerical results agree with the above prediction.

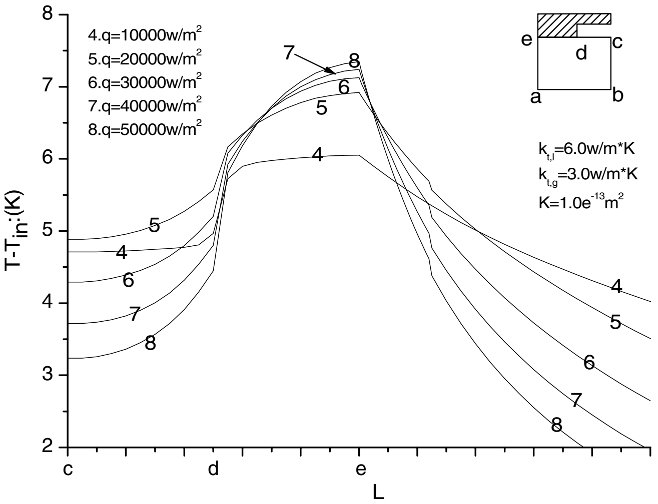

Fig. 11. Profiles of temperature on local boundary of steady states at different heat fluxes.

As shown in Figs. 10b and 11, profiles of temperature along boundary of steady states at low or moderate heat fluxes have different patterns compared with the mono-pattern of profiles of pressure at different heat fluxes. Temperature increases along radial direction from the entrance to the heated fin while there are two-dimensional patterns of isotherms in the vicinity of heated fins and grooves and there is a local relative low-temperature region near the

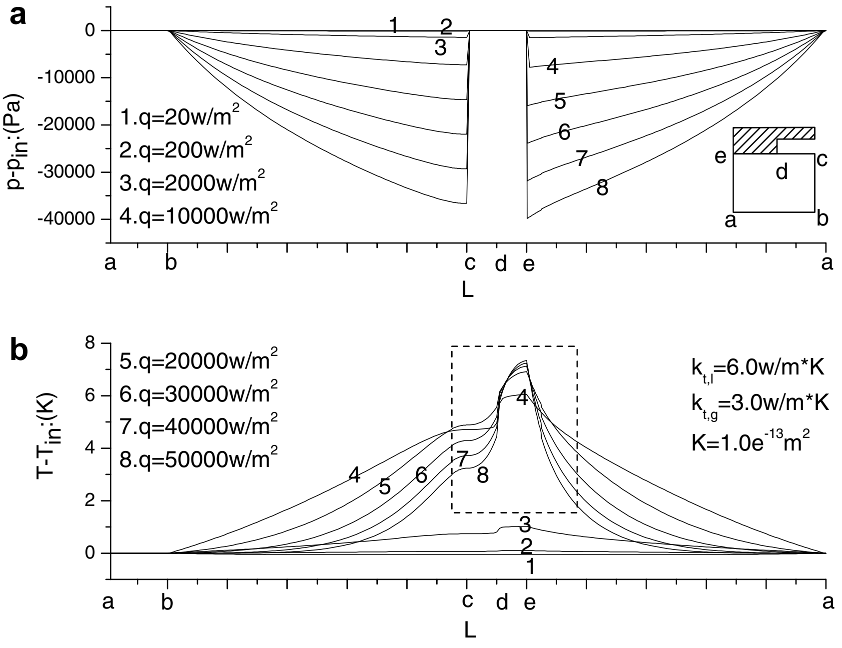

Fig. 10. Profiles of (a) pressure and (b) temperature along boundary of steady states at different heat fluxes.

interface at the symmetric center of the vapor groove. However, temperature does not increase monotonously everywhere in the wick with heat fluxes increasing. At low heat fluxes, such as lower than $q = 10\,000\ \mathrm{W/m^2}$, effect of heat conduction of the porous structure is stronger than effect of convection of the cool working liquid everywhere in the wick. So temperature increases monotonously everywhere in the wick with the heat flux increasing and the profile of temperature maintains the same slope in almost all regions at a certain heat flux. The heat leak on the entrance, determined by the slope of profile of temperature on the boundary a–b, increases with the heat flux increasing. At moderate heat fluxes, such as higher than $q = 10\,000\ \mathrm{W/m^2}$, effect of heat conduction of the porous structure is stronger than effect of convection of the cool working liquid in the vicinity of heated fins and weaker than effect of convection in the bottom region while effect of heat conduction is comparative to effect of convection in other regions. So temperature in the vicinity of heated fins increases with the heat flux increasing but temperature elsewhere decreases. The slopes of profiles of temperature become steeper and steeper from the bottom to the top so that there lie a high-temperature region at the top and a low-temperature region at the bottom with a transitional region between them. On the one hand, higher heat flux leads to the thinner high-temperature region with higher temperature, the larger low-temperature region with lower temperature and the steeper slope of the profile of temperature in the transitional region. On the other hand, higher heat flux leads to less heat leak on the entrance. These results about profiles of temperature in porous media agree well with the experimental results in [11]. It is proved that effect of convection of the working fluid in wicks on the distribution of temperature is so important that the results with convection neglected do not bring forth the true distribution of temperature. Due to effect of convection, lower temperature is kept in most regions at higher heat flux except in the vicinity of heated fins. So convection helps to increase the safety of LHPs.

As shown in Fig. 12a, movement of interfaces at low or moderate heat fluxes does not vary monotonously. At extremely low heat fluxes such as $q = 20\ \mathrm{W/m^2}$, vapor is constrained in some isolated micro-bubbles in most time with the intermittent passage to the vapor groove. No enough energy is supplied to maintain a full-time passage through which vapor can move out into the vapor groove so that the phenomenon of "convergency–eruption–convergency" exists. So the fluxes at extremely low heat fluxes are oscillatory with time, such as the flux at $q = 20\ \mathrm{W/m^2}$ shown in Fig. 9. There lies a full-time passage, called a vapor blanket in [10,11], between the heated fin and the liquid-saturated zone in porous media with the heat flux increasing, which is proved experimentally or theoretically in [10,11] no matter whether the vapor blanket is macroscopic or microscopic. The heat flux "turns on" the LHP in aspects of not only evaporation but also the working fluid flowing. According to the above discussion, there are three competing dynamic and thermodynamic processes: evaporation, heat conduction of the porous structure and convection of the cool working liquid. Because the behavior of the interface includes both the position of the interface and the curvature of menisci on the interface, effect of the interaction between the flow field and the liquid–vapor interface lies in both above aspects. Heat conduction of the porous structure transfers heat from the heated fin to the interface while convection of the cool

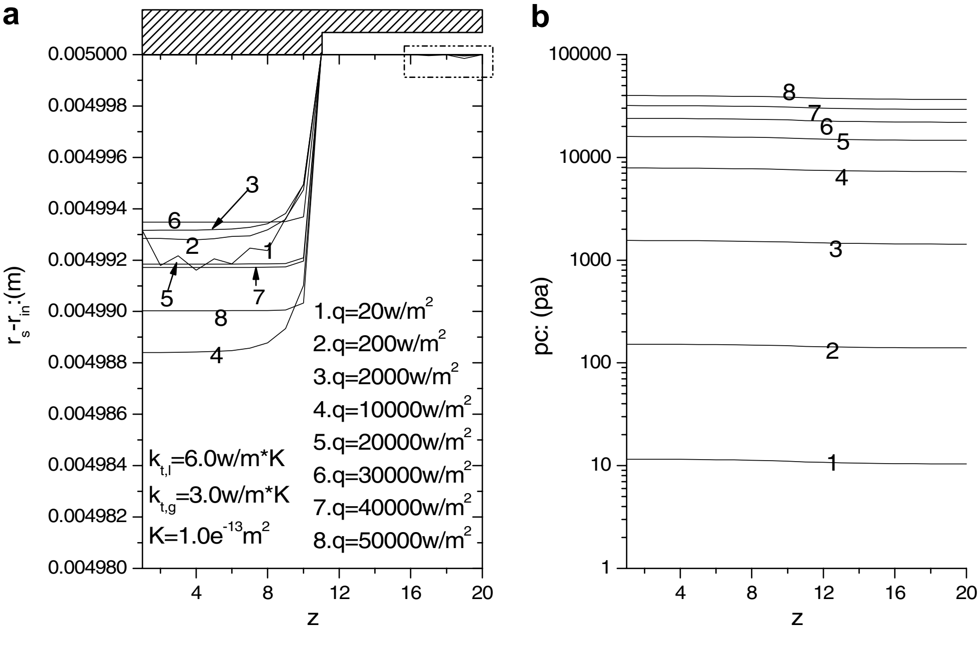

Fig. 12. Effect of heat flux on (a) the position of the interface and (b) capillary forces on the interface (note that there is a log scale in the ordinate of (b) and that the difference of capillary forces on different sections of the interface at a certain heat flux is too small to be displayed in (b)).

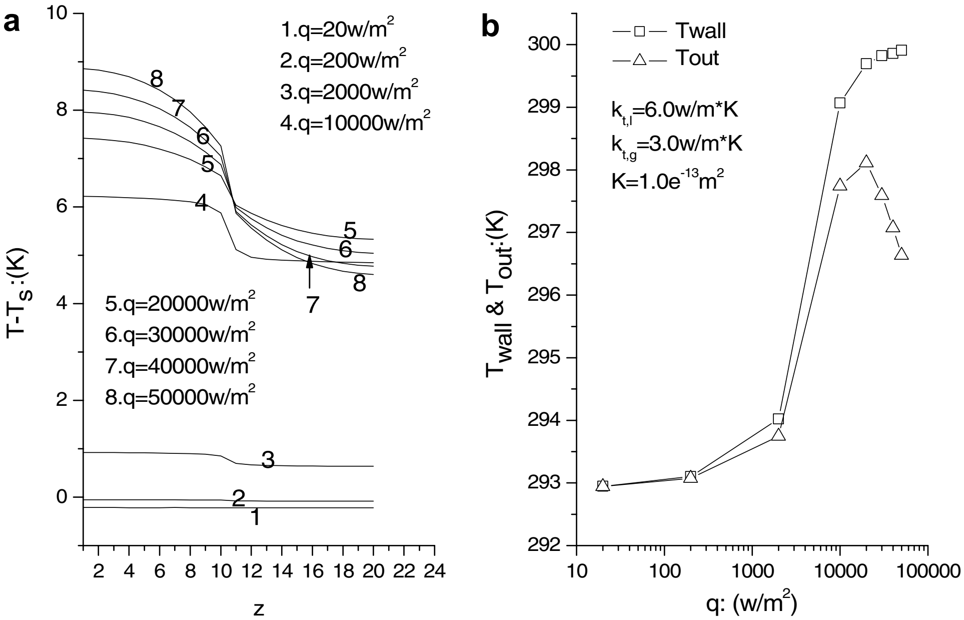

Fig. 13. Effect of heat flux on (a) the superheating temperature on the interface $T - T_s$, (b) mean fin temperature T_{wall} and mean outlet temperature T_{out}.

working liquid transports liquid from the entrance to the interface. Evaporation makes use of both heat and liquid on the interface. The behavior of the interface is a result of the combining effect of evaporation, heat conduction and convection. The vapor blanket invades more deeply into the wick when effect of evaporation and heat conduction is stronger than effect of convection, and it is pushed back when effect of evaporation and heat conduction is weaker than effect of convection. The vapor blanket with effect of convection is thinner than that without effect of convection at every heat flux so that convection could not be neglected in order to bring forth the true phenomenon in a capillary porous structure at heat fluxes. The thickness of vapor blankets at low or moderate heat fluxes is too small to be visually observed in experiments, which agree with the results in [11].

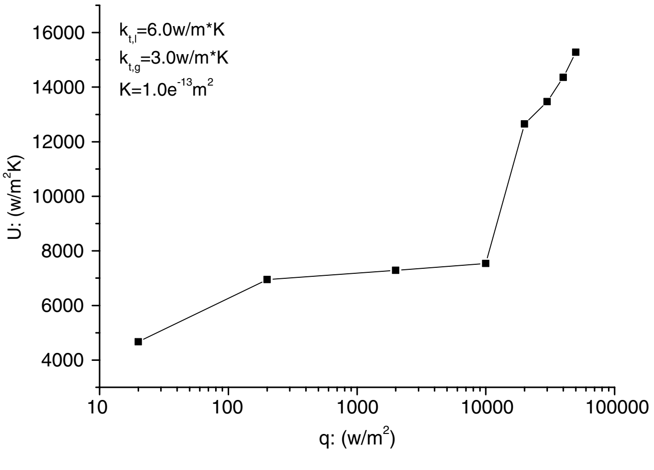

Fig. 14. Wick's total heat transfer coefficient at different heat fluxes.

Superheating temperature on the interface $T - T_s$, mean fin temperature T_{wall} and mean outlet temperature T_{out} at different heat fluxes are shown in Fig. 13. Due to effect of capillary force on the liquid–vapor thermodynamic equilibrium as predicted by the Kelvin equation (13), the superheating temperature is related to the difficulty of organizing evaporation in the capillary porous media. On the one hand, the superheating temperature increases with the heat flux increasing. On the other hand, different superheating temperatures are on different sections of the interface. The higher the heat flux is, the more evident the difference of superheating temperatures on the interface is. Greater superheating temperature on the section closer to the center of the heat source leads to more difficult evaporation. As shown in Fig. 13b, mean fin temperature increases monotonously with the heat flux increasing but mean outlet temperature increases to a peak and then drops with the heat flux increasing, which is explained in the above section.

For engineers, wick's total heat transfer coefficient is the primary interest. It is calculated in the following formula [11]:

$$U = \frac{q}{T_{wall} - T_{out}}, \tag{18}$$

where U is wick's total heat transfer coefficient. As shown in Fig. 14, the total heat transfer coefficient increases monotonously with the heat flux increasing, which agrees with the experimental results in [11]. These heat transfer devices depending on evaporation and convection of the cool working liquid have large capacity of heat transfer and higher total heat transfer coefficient at higher heat flux. Evaporation leads to large capacity of heat transfer with a little working fluid. Convection of the cool working liquid protects most regions of the wick even at high heat fluxes. All these excellences make it applied to more and more engineering regions.

5. Conclusions

An axisymmetric two-dimensional mathematical model of the cylindrical evaporator's wick of LHPs is developed to simulate heat transfer with flow and evaporation in the capillary porous structure. Effect of the interaction between the flow field and the liquid–vapor interface on the position of the interface and the curvature of menisci is adequately considered in this model. The flow field of transient and steady states with effect of wick's cylindrical shape is obtained at low or moderate heat fluxes. The dynamic and thermodynamic behavior is discussed. The auto-driving mechanism of "inverted meniscus type" evaporators is validated.

Evaporation occurs everywhere on the interface with different intensity of evaporation on different sections of the interface. It vaporizes more strongly in the region closer to the center of the heat source. There lies a steady vapor blanket between heated fins and the liquid-saturated zone in porous media for a definite interval of heat fluxes except that there lie isolated micro-bubbles in the vicinity of heated fins at extremely low heat fluxes. The behavior of the interface is a result of the combining effect of evaporation, heat conduction of the porous structure and convection of the cool working liquid. The vapor blanket invades more deeply into the wick when effect of evaporation and heat conduction is stronger than effect of convection, and it is pushed back when effect of evaporation and heat conduction is weaker than effect of convection. In capillary porous media, the interface adapts itself to steady states at different heat fluxes automatically by two means: It changes the curvature of menisci or its position in porous media to adjust the flux of the working fluids.

Convection of the cool working fluid influences strongly the flow field and interface in capillary porous media. Due to effect of convection, lower temperature is kept in most regions at higher heat flux except in the vicinity of heated fins, which helps to increase the safety of LHPs. The vapor blanket with effect of convection is thinner than that without effect of convection at every heat flux. Investigation with convection neglected can not bring forth the true phenomenon of flow, heat transfer and evaporation in capillary porous media.

Heat flux influences strongly the steady flow field and interface as well as wick's performances. In the allowed range of heat fluxes, Higher heat flux leads to stronger convection and more intense evaporation, which helps to increase the device's safety by keeping lower temperature in most regions except in the vicinity of heated fins and increases wick's total heat transfer coefficient.

Acknowledgements

The authors acknowledge the support of Chinese Academy of Space Technology (CAST), and Chinese Academy of Science (CAS) with a dean excellent fund.

References

[1] T. Kaya, T.T. Hoang, Mathematical modeling of loop heat pipes and experimental validation, J. Thermophys. Heat Transfer 13 (3) (1999) 314–320.

[2] T. Kaya, T.T. Hoang, Mathematical modeling of loop heat pipes with two-phase pressure drop, AIAA paper No.99-3448, 1999.

[3] T. Hoang, J. Ku, Hydrodynamic aspects of capillary pumped loops, SAE paper No.961435, 1996.

[4] J. Ku, Operating characteristics of loop heat pipes, SAE paper No.1999-01-2007, 1999.

[5] E. Pouzet, J.L. Joly, V. Platel, J.Y. Grandpeix, C. Butto, Dynamic response of a capillary pumped loop subjected to various heat load transients, Int. J. Heat Mass Transfer 47 (10-11) (2004) 2239–2316.

[6] H.X. Zhang, G.P. Lin, T. Ding, W. Yao, X.G. Shao, R.G. Sudalov, Yu. F. Maidanik, Investigation of startup behaviors of a loop heat pipe, J. Thermophys. Heat Transfer 19 (4) (2005) 509–518.

[7] L.L. Vasiliev, Heat pipes in modern heat exchanges, Appl. Therm. Eng. 25 (2005) 1–19.

[8] Yu. F. Maydanik, Loop heat pipes, Appl. Therm. Eng. 25 (2005) 635–657.

[9] K.T. Feldman, D.L. Noreen, Design of heat pipe cooled laser mirrors with an inverted meniscus evaporator wick, AIAA paper No.92-0148, 1980.

[10] D. Khrustalev, A. Faghri, Heat transfer in the inverted meniscus type evaporator at high heat fluxes, Int. J. Heat Mass Transfer 38 (16) (1995) 3091–3101.

[11] T.S. Zhao, Q. Liao, On capillary-driven flow and phase-change heat transfer in a porous structure heated by a finned surface: measurements and modeling, Int. J. Heat Mass Transfer 43 (2000) 1141–1155.

[12] A.S. Demidov, E.S. Yatsenko, Investigation of heat and mass transfer in the evaporation zone of a heat pipe operating by the 'inverted meniscus' principle, Int. J. Heat Mass Transfer 37 (14) (1994) 2155–2163.

[13] C. Figus, Y. Le Bray, S. Bories, M. Prat, Heat and mass transfer with phase change in a porous structure partially heated: continuum model and pore network simulation, Int. J. Heat Mass Transfer 42 (1999) 2557–2569.

[14] A.R. Takahashi, A.A. Oliveira, E. Bazzo, Analysis of heat and mass transfer with phase change in the porous wick of a capillary pump, in: The 7th International Heat Pipe Symposium, October 12–16, 2003, Jeju Korea.

[15] K.S. Udell, Heat transfer in porous media heated from above with evaporation, condensation and capillary effects, ASME J. Heat Transfer 105 (1983) 485–492.

[16] D.L. Zeng et al., Engineering Thermodynamics, Higher Education Press, Beijing China, 1985, pp. 191–198 (in Chinese).

[17] X.Y. Kong, Advanced Fluid Mechanics in Porous Media, USTC Press, Hefei China, 1999, pp. 38–39, pp. 45–49 (in Chinese).

[18] W.Q. Tao, Neoteric Advance in Numerical Heat Transfer, Science Press, Beijing China, 2001, pp. 233–237, pp. 283–286 (in Chinese).

[19] B.X. Wang, Heat and Mass Transfer in Engineering, vol. 2, Science Press, Beijing China, 1998, pp. 342–347 (in Chinese).